JACS
JOURNAL OF THE AMERICAN CHEMICAL SOCIETY
pubs.acs.org/JACS
Article

Aquafoldmer-Based Aquaporin-like Synthetic Water Channel

Jie Shen, Ruijuan Ye, Alyssa Romanies, Arundhati Roy, Feng Chen, Changliang Ren, Zhiwei Liu, and Huaqiang Zeng*

Cite This: J. Am. Chem. Soc. 2020, 142, 10050−10058
Read Online
ACCESS | Metrics & More | Article Recommendations | Supporting Information

ABSTRACT: Synthetic water channels were developed with an aim to replace aquaporins for possible uses in water purification, while concurrently retaining aquaporins' ability to conduct highly selective superfast water transport. Among the currently available synthetic water channel systems, none possesses water transport properties that parallel those of aquaporins. In this report, we present the first synthetic water channel system with intriguing aquaproin-like features. Employing a "sticky end"-mediated molecular strategy for constructing abiotic water channels, we demonstrate that a 20% enlargement in angstrom-scale pore volume could effect a remarkable enhancement in macroscopic water transport profile by 15 folds. This gives rise to a powerful synthetic water channel able to transport water at a speed of ~3 × 10^9 H_2O s^{-1} $channel^{-1}$ with a high rejection of NaCl and KCl. This high water permeability, which is about 50% of aquaporin Z's capacity, makes channel **1** the fastest among the existing synthetic water channels with high selectivity.

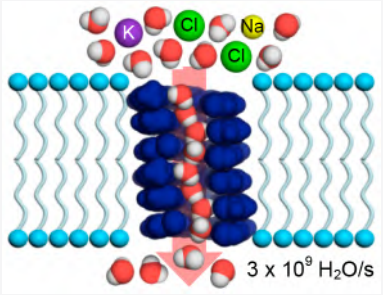

Downloaded via NATL UNIV OF SINGAPORE on June 25, 2020 at 03:19:44 (UTC).
See https://pubs.acs.org/sharingguidelines for options on how to legitimately share published articles.

INTRODUCTION

With 4 billion people globally suffering from severe water scarcity,[1] meeting mankind's increasing demand for clean water is one of the most difficult and important challenges of this century.[2,3] This vital challenge has made the reverse-osmosis (RO) membrane technique the dominant process for clean water production, currently generating 100 million tons of desalinated water per day from the oceans, the Earth's most abundant water source.[4−6] Its high energy consumption however limits its widespread adoption.

Aquaporins (Aqps) are a specialized family of protein-based membrane channels for mediating superfast water transport across a lipid membrane, with complete rejection of both salts and protons.[7−9] In particular, Aquaporin Z (AqpZ), which exhibits a water transport rate of ~6 × 10^9 H_2O s^{-1} $channel^{-1}$,[10,11] has since greatly invigorated both academia and industry to investigate possible uses of AqpZ-based biomimetic membranes in low-energy water treatments for medical (e.g., kidney dialysis) as well as industrial and municipal desalting applications (seawater desalination, wastewater remediation, etc.).[12−19]

On the other hand, AqpZ's high performance in water transport has also motivated researchers to develop simpler versions, i.e., bioinspired synthetic water channels based on small molecules[20−28] or carbon nanotubes (CNTs)[29] for replacing AqpZ in its intended applications. For this purpose, preserving AqpZ's high permeability and selectivity in water transport is an indispensable prerequisite for practical applications involving synthetic water channels. This is and so far proves to be challenging. In fact, among the existing synthetic water channels reported by others,[20−29] while CNTs with extraordinarily high water permeability are not selective in water transport,[29] those highly selective synthetic water channels[20−27] transport water molecules at low rates of <4 × 10^7 H_2O s^{-1} $channel^{-1}$, which are <1% of water transport capacity of AqpZ. Further, the recently reported highly selective and fast transmembrane water transport was not conducted through the pore of the channel molecules, which actually is too small for a water molecule.[28] Rather, it was mediated completely by membrane defects induced by the molecular clustering effect. In addition, we recently elaborated polypyridine-based foldamer channels able to conduct water transport at 1.6 × 10^9 H_2O s^{-1} $channel^{-1}$ (~27% of AqpZ's capacity in water transport).[30] Presently, synthetic water channels, which simultaneously recapitulate two hallmarks of AqpZ (e.g., high water permeability and high salt rejection), still remain unknown.

Here we report our surprising discovery, via a "sticky" end-mediated construction strategy[18] (Figure 1a), of an aromatic aquafoldamer-based synthetic water channel (**1**, Figure 1b). With an internal hollow cavity of ~2.8 Å across that matches the size of AqpZ's central pore (2.8 Å), channel **1** displays high water transport (~3 × 10^9 H_2O s^{-1} $channel^{-1}$) and high rejection of salts such as NaCl and KCl. This high water permeability represents a more than 70-fold improvement over all synthetic water channels with high salt rejections elaborated by others[20−27] or an 88% enhancement over polypyridine

Received: February 20, 2020
Published: May 6, 2020

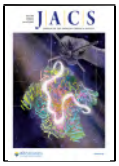

ACS Publications
© 2020 American Chemical Society

https://dx.doi.org/10.1021/jacs.0c02013
J. Am. Chem. Soc. 2020, 142, 10050−10058

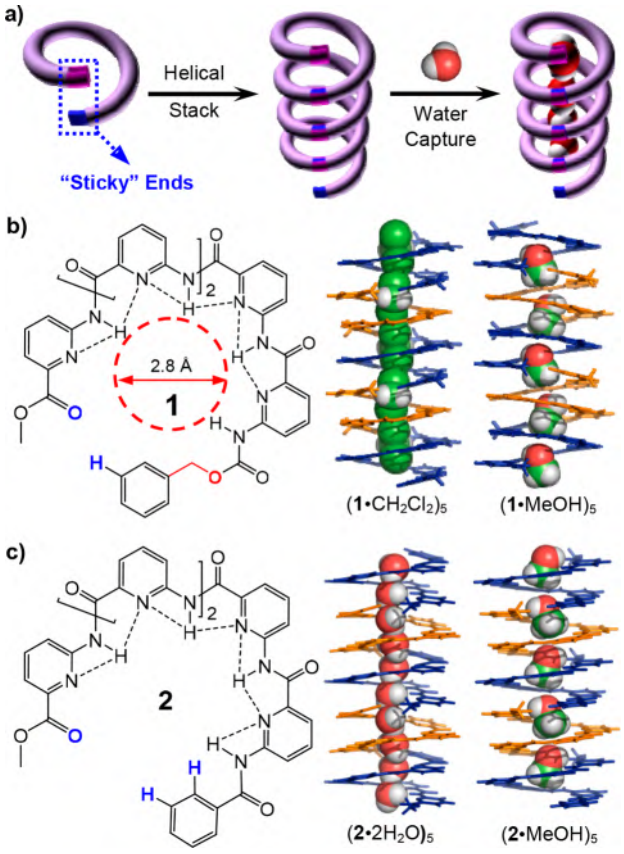

Figure 1. Molecular design and crystal structures of aquafoldamer-based synthetic water channels. (a) A "sticky end"-mediated molecular strategy for creating self-assembled 1D nanotubes for water transport. (b) Chemical and crystal structures of **1**, encapsulating 1D chain of dichloromethane (CH_2Cl_2) or methanol (MeOH)[31] molecules. (c) Chemical and crystal structures of **2**, encapsulating the 1D chain of water or MeOH molecules. Sticky ends that are involved in forming intermolecular H-bonds are highlighted in blue.

channels recently reported by us,[30] making **1** the first example of synthetic water channel that possesses attractive aquaporin-like features in water transport. Interestingly, with respect to **1**, which binds to water more weakly, structurally similar channel **2** (Figure 1c), possessing a high similarity in interior surface functionality and a mere reduction of ~20% in internal pore volume, exhibits a 15-fold decrease in the water transport rate. Highlighting anomalous water transport behaviors in the angstrom-scale hollow pore, these two channels also constitute one ideal pair with contrasting performances for testing existing and emerging computational algorithms in accurately predicting water transport properties of narrow pores at or below the nanometer scale.

RESULTS AND DISCUSSION

Differential Binding Affinities of Aquafoldamers 1 and 2 toward Water Molecules. Inspired by the Aqps' central pore opening of ~2.8 Å in diameter, we recently designed and reported a class of H-bonding-induced helically folded pyridine foldamers, which are able to recognize water molecules and thus termed aquafoldamers. These folded aquafoldamers possess a cavity of ~2.8 Å across defined by the inward-pointing amide H atoms.[18] With their cavity interior decorated by pyridine N atoms and amide H atoms that serve as H-bond acceptors and donors for water binding, aquafoldamers such as **2** (Figure 1c) could accommodate two water molecules. In 2012, we introduced electrostatically complementary "sticky ends" at the helical two ends of short oligomers (e.g., **1**[31] and **2**[25]), forming numerous weak intermolecular H-bonds to seamlessly cross-link short helices **1** or **2** into long 1D nanotubes in solid state (Figure 1b,c).

Our detailed studies on nanotube-forming **1**[31] and **2**[25] reveal their differential binding patterns toward H_2O, MeOH, and CH_2Cl_2 molecules. For **1**, the binding increases in the order of CH_2Cl_2 < H_2O < MeOH; for **2**, the order becomes CH_2Cl_2 < MeOH < H_2O.[18] In other words, our early attempts to grow water-containing crystals yielded crystals $(\mathbf{2}\cdot 2H_2O)_n$. For **1**, we only obtained crystals of $(\mathbf{1}\cdot CH_2Cl_2)_n$ or $(\mathbf{1}\cdot MeOH)_n$, not $(\mathbf{1}\cdot 2H_2O)_n$.

Superfast Transmembrane Water Transport by 1. We initially thought that, when incorporated into a lipid bilayer, 1D stacks of $(\mathbf{2}\cdot 2H_2O)_n$ should facilitate faster single file water movement across a membrane under an osmotic pressure than **1**, which favors the guest molecules of MeOH over water (Figure 1b).

In this work, we quantitatively compared water transport properties of aquafoldamers **1** and **2**, with **2** binding to water more strongly than **1**, using a stopped flow instrument that allows fast kinetics on a millisecond time scale to be evaluated properly for determining water permeability. Given a hydrophobic thickness of 28 Å for DOPC (1,2-dioleoyl-*sn*-glycero-3-phosphocholine lipid) membrane[32] and a crystallographyically determined helical height of ~5 Å for **1** or **2**, six molecules of **1** or **2** are required to span the hydrophobic membrane region of DOPC. Thus, DOPC lipids and **1** or **2** were mixed at different molar ratios of 300:1 to 1300:1 in chloroform to give lipid/channel molar ratios of 1800:1 to 7800:1, which were made into ~120 nm large unilamellar vesicles (LUVs) in a HEPES buffer (10 mM HEPES, 100 mM NaCl, pH = 7.0). Exposure of these LUVs to an equal volume of a hypertonic 300 mM sucrose osmolyte in the same HEPES buffer results in water efflux and vesicle shrinkage, which in turn leads to increased light scattering intensity (Figure 2a). From changes in light scattering as a function of time, the water permeability (P_f in units of cm/s) of vesicles in the absence and presence of water channels can be extracted. With the assumption that each self-assembled channel comprises six molecules as well as based on the channel insertion efficiency and actual lipid concentration after extrusion (Figures S2 and S3 and Table S1), we calculated the single-channel permeability (P_w in units of cm^3/s) for **1** and **2**.

Surprisingly, channel **1**, which was believed to be slower in water transport as originally conceived from its lower affinity to water molecules when compared to **2**, turns out to induce much faster water flow across a membrane than **2**. Its water permeability ranges from 6.53 ± 0.45 to 9.23 ± 0.26 × 10^{-14} cm^3/s at lipid/channel molar ratios of 3000:1 to 7800:1. A much lower permeability of 3.90 ± 0.18 × 10^{-14} cm^3/s at a lipid/channel ratio of 1800:1 (e.g., high channel density) arises from the channel's low solubility in the DOPC membrane. The highest permeability value of 9.23 ± 0.26 × 10^{-14} cm^3/s determined at a lipid/channel molar ratio of 4200 corresponds to a superfast water transport of 3.0 × 10^9 H_2O s^{-1} $channel^{-1}$.[33] This value is 15 times that of channel **2** (Figure 2b) and more than 70 times those of the other types of highly selective synthetic water channels.[22−24]

https://dx.doi.org/10.1021/jacs.0c02013
J. Am. Chem. Soc. 2020, 142, 10050−10058

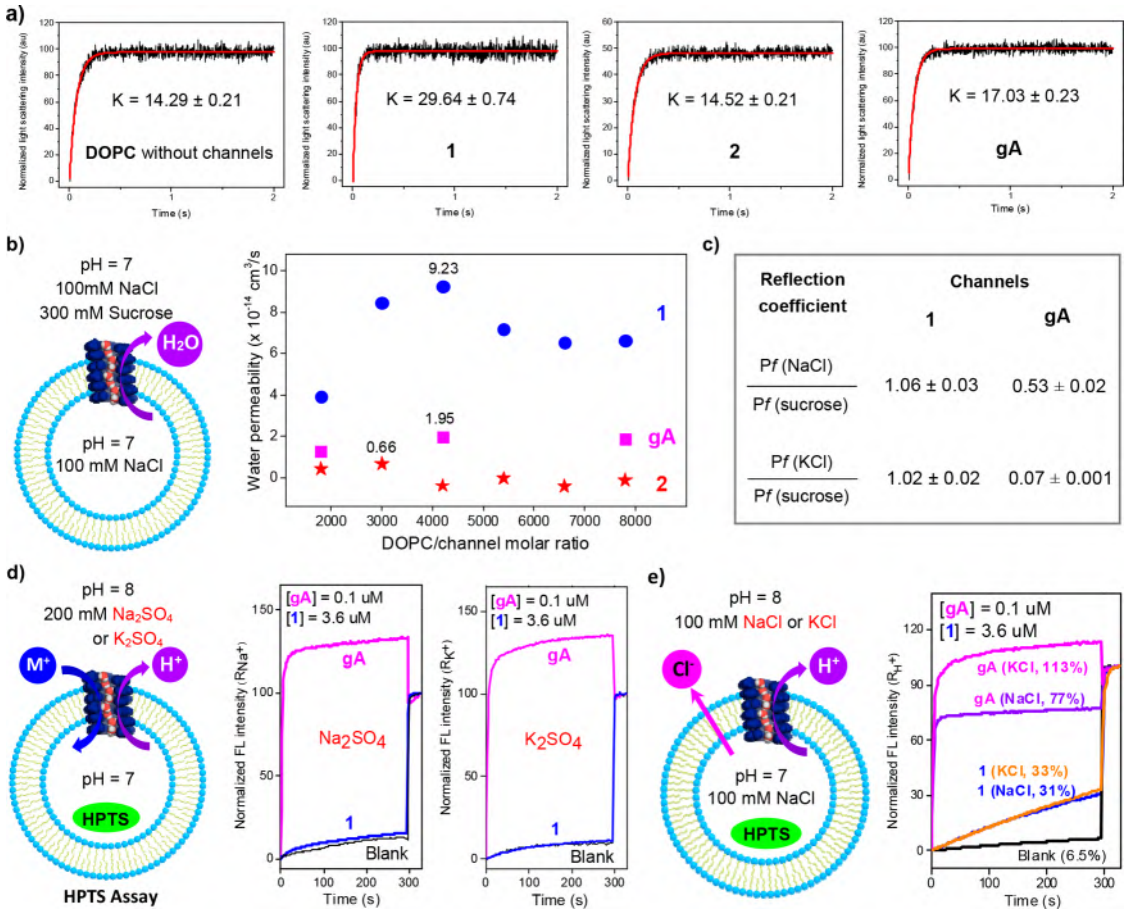

Figure 2. Water permeability of channels **1**, **2**, and gA and transport selectivity determined for **1**. (a) Representative water transport curves for DOPC only, **1**, **2**, and gA obtained using a stopped flow apparatus at a lipid/channel molar ratio of 4200:1. Exponential coefficients (K) were obtained by fitting the data into the equation of $y = A\exp(-kx) + y0$. (b) LUV-based hypertonic conditions (300 mM sucrose) for water permeability measurement for **1**, **2**, and gA at different lipid/channel molar ratios, with data averaged in triplicate. (c) Water permeability measured using three types of hypertonic conditions (300 mM sucrose, 250 mM NaCl, or 250 mM KCl), suggesting complete and incomplete salt rejections by **1** and gA, respectively. (d) HPTS-based LUV assays under high ionic concentration gradients, confirming that **1** does not transport both Na^+ and K^+ ions. (e) HPTS-based LUV assays under a proton gradient, suggesting that $(\mathbf{1}{\cdot}2H_2O)_n$ is not optimized for transport of Na^+ or K^+ ions with respect to gA. Instead, it transports protons with slow passive diffusion of Cl^- to maintain the charge balance. gA = gramicidin A; HPTS = 8-hydroxypyrene-1,3,6-trisulfonic acid.

Channel **2** exhibits the highest water permeability of 0.66 ± 0.12 × 10^{-14} cm^3/s (2.2 × 10^8 H_2O s^{-1} $channel^{-1}$) at a lipid/channel molar ratio of 3000:1, followed by 0.41 ± 0.15 × 10^{-14} cm^3/s at a lipid/channel molar ratio of 1800:1 (Figure 2b).[30] At higher lipid/channel molar ratios of >4000:1, no appreciable water transport can be detected for **2**, likely because the channel density is so low that the background water permeability becomes dominated over those by **2**.

In comparison, gramicidin A (gA) gives water permeabilities of 1.28 ± 0.03 to 1.95 ± 0.11 × 10^{-14} cm^3/s (4–6 × 10^8 H_2O s^{-1} $channel^{-1}$, Figure 2b),[30] which are in good agreement with a value of 1.6 ± 0.3 × 10^{-14} cm^3/s reported by Pohl.[34]

High Selectivity in 1-Mediated Water Transport. Fast water transport is just one aspect of naturally occurring AqpZ. Another significant aspect of AqpZ is its high selectivity in water transport, rejecting both salts (NaCl and KCl) and protons. For practical applications in water treatment, high selectivity is as important as, if not more important than, water transport rate. We therefore designed four sets of lipid bilayer experiments to examine the selectivity of **1**-mediated water transport.

We first compared the water permeability (P_f) values of vesicles in the presence of three different hypertonic conditions (300 mM sucrose that does not permeate the membrane, 150 mM NaCl and 150 mM KCl). For channel **1**, background-subtracted P_f values averaged in triplicate for sucrose, NaCl and KCl at a lipid/channel ratio of 4200:1 are 163.00 ± 1.58, 174.57 ± 7.96, and 167.13 ± 5.61 μm/s, respectively. The reflection coefficients, defined as the ratio of the P_f value of salt over that of sucrose, are 1.07 ± 0.04 for NaCl and 1.03 ± 0.02 for KCl (Figure 2c). These reflection coefficients, which differ insignificantly from 1.00, confirm that **1** achieves high rejection of both NaCl and KCl,[35] as a result of the aquapore's narrow size of 2.8 Å that is just big enough for a single water molecule and its lack of binding elements for liberating ions from their hydration shells. For gA, the corresponding reflection coefficients decrease to 0.53 ± 0.02 for NaCl and to 0.07 ± 0.001 for KCl, which are fully consistent with the high permeability of gA toward both Na^+ and K^+ ions and high salt rejection capacity of **1**.

Next, we monitored transport of Na^+ and K^+ ions across the bilayer membrane in the presence of **1** or gA using standard fluorescence assays, incorporating pH-sensitive fluorescent

https://dx.doi.org/10.1021/jacs.0c02013
J. Am. Chem. Soc. 2020, 142, 10050−10058

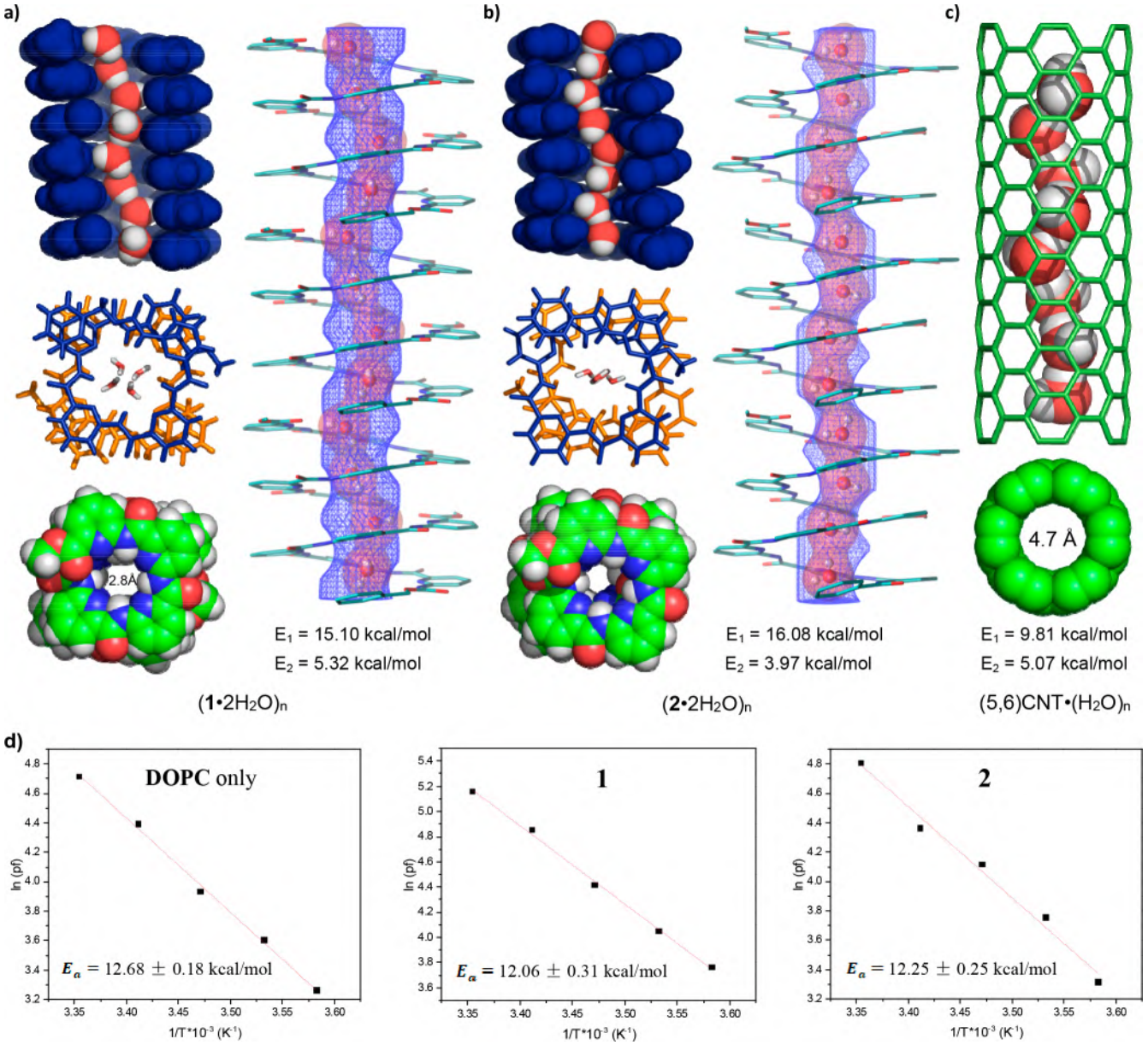

Figure 3. Water-containing crystal structures of **1** and**2** as well as the computed structure of (5,6)CNT, the corresponding volume maps and the average binding energy between the wall interior and a water molecule from the water chain (E_1) and average H-bond energy in the water chain (E_2). (a) Crystal structure of $(\mathbf{1}{\cdot}2H_2O)_n$ and energies of E_1 and E_2 calculated at the level of ωB97X/6-31G++(2d,p). (b) Crystal structure of $(\mathbf{2}{\cdot}2H_2O)_n$ and energies of E_1 and E_2. (c) Water-containing structure of (5,6)CNT$\cdot(H_2O)_n$, having a cavity diameter of 4.7 Å, and energies of E_1 and E_2. The pore volume maps (blue mesh) shown in parts a and b were obtained using the VolMap method in VMD in the format of 3D density grid (cubic grid size = 0.3 Å, diameter of the enclosing cylinder = 4.4 Å, grid densities of <0.2 considered unoccupied). Using this method, the internal hollow cavity volume in $(\mathbf{1}{\cdot}2H_2O)_n$ is estimated to be >20 vol % larger than that in $(\mathbf{2}{\cdot}2H_2O)_n$. The volume maps (red) of the water chain (grid densities >0.5 considered unoccupied) were also shown in parts a and b. (d) Arrhenius plots of the water permeability as a function of temperature (6−25 °C) for DOPC only, **1** and **2** for determining activation energies (E_a) averaged over three runs.

HPTS dye under high ionic concentration gradients (200 mM Na_2SO_4 or K_2SO_4, Figure 2d). Compared to rapid increases in fluorescence intensity by >120% within 10 s achieved by Na^+/K^+-permeable gA at 0.1 μM ([channel] = 0.05 μM), negligible changes of <3% induced by **1** at 3.6 μM ([channel] = 0.6 μM) for both Na^+ and K^+ ions clearly indicate that neither ions could permeate the aquapores formed by **1**. Using the chloride-sensitive SPQ (6-methoxy-*N*-(3-sulfopropyl)-quinolinium)) assay (Figure S1),[36] we observed rapid quenching of SPQ dye by chloride channel **L8**[32] at 0.5 μM ([channel] = 0.1 μM) but not by channel **1** at the same channel concentration. These data therefore exclude Cl^- anion as the molecular species transportable by **1**. Increasing the concentration of Na_2SO_4 to 300 mM, which is the concentration of Na^+ ions found in the seawater, gave the same results (Figure S5a).

Additionally, at a channel concentration 12 times that of gA (0.6 μM vs 0.05 μM, Figure 2e), **1** achieves low fractional transport activities of ∼33% within 300 s, which are much slower than gA eliciting transport activities of >70% in just 10 s. This observation is consistent with the data presented in Figure 2c,d and Figure S5, demonstrating that, unlike gA that

https://dx.doi.org/10.1021/jacs.0c02013
J. Am. Chem. Soc. 2020, 142, 10050−10058

can transport H^+, Na^+, and K^+ ions, **1** does not transport both Na^+ and Cl^- ions. As such, the **1**-mediated efflux of protons can only be accompanied by the slower passive diffusion of Cl^- anion across membrane, rather than channel-mediated fast transport of Na^+ or K^+ ions as in gA, in order to maintain the charge balance of the system. Using the same HPTS assay in Figure 2e, we carried out proton transport study in the presence of proton carrier FCCP (carbonyl cyanide-4-(trifluoromethoxy)phenylhydrazone). The fact that the presence of FCCP did not enhance the proton transport activity suggests the passive diffusion of Cl^- anions to be the rate-limiting step (Figure S5b).

Factors Underlying 1-Mediated Superfast Water Transport. Encouraged by the superfast water transport mediated by **1** for which we previously did not succeed in obtaining crystals containing only water molecules inside the hollow aquapores, we set out to explore more crystal growth conditions. Given a cuboid geometry of 3.2 Å (W) × 5.4 Å (L) × 6.5 Å (H) for the acetone molecule that cannot fit into the narrow cavity of ~3.2 Å defined by the interior N atoms in **1**, we thought that diffusion of mixed solvents composed of acetone and water into **1**-containing CH_2Cl_2 solution may yield water-containing crystals. Indeed, after testing more than 10 combinations involving varied volumetric ratios and concentrations of **1** in CH_2Cl_2, we obtained water-containing quality crystals, via slow diffusion of 0.5 mL of acetone/water (1:2, v:v) into 0.4 mL of CH_2Cl_2 solution having 1 mg of **1** over a week at room temperature. In the solid state, water molecules are one dimensionally H-bonded and aligned inside hollow aquapores generated via the helical stacking of numerous molecules of **1** (Figure 3a).

Structural and energetic analyses of $(\mathbf{1}\cdot 2H_2O)_n$ and $(\mathbf{2}\cdot 2H_2O)_n$[25] reveal three noticeable dissimilarities in terms of the volume of the hollow aquapore, wettability of the pore interior surface, and energy of H-bonds in the water chain. Structurewise, **1** has one more C atom and one more O atom at the amino end than **2**. These two additional atoms force the end benzene group in **1** to point more away from the center of the pore interior than the end benzene group in **2** (Figure S4a). Subsequent helical packing via sticky ends generates a cylindrical aquapore of 2.8 Å across for $(\mathbf{1}\cdot 2H_2O)_n$ and a roughly cuboidal aquapore of 2.1 Å × 2.7 Å for $(\mathbf{2}\cdot 2H_2O)_n$. Inspection of crystal structures of $(\mathbf{1}\cdot 2H_2O)_n$, $(\mathbf{1}\cdot MeOH)_n$ and $(\mathbf{1}\cdot CH_2Cl_2)_n$ shows that the same type of cylindrical aquapore with the same cavity size is maintained across all three structures (Figure 1b and Figure S4b), suggesting a hollow cavity of 2.8 Å across is sufficiently spacious and robust to accommodate chains of water, methanol, and dichloromethane molecules. Using the 3D density grid generated by the VolMap method in VMD (cubic grid size = 0.3 Å, diameter of the enclosing cylinder for pore volume calculation = 4.4 Å, and grid densities of <0.2 inside the enclosure considered unoccupied), the hollow cavity in $(\mathbf{1}\cdot 2H_2O)_n$ is estimated and consistently more spacious than that in $(\mathbf{2}\cdot 2H_2O)_n$ by >20 vol % (see volume maps in Figure 3a,b and Table S2). As such, in a larger hollow aquapore contained in $(\mathbf{1}\cdot 2H_2O)_n$, water molecules must possess higher degrees of translational and rotational freedoms, certainly contributing to the enhanced water flow rate through the pore.

Energywise, the functional groups lining the interior of the pore surface in $(\mathbf{1}\cdot 2H_2O)_n$ form six H-bonds per water pair molecule with the water chain (Figure S7a), contributing an average binding energy (E_1) of 15.10 kcal/mol per water molecule at the level of ωB97X/6-31G++(2d,p), which is about 6% smaller than that provided by **2** (16.08 kcal/mol), having six H-bonds per water pair (Figure S7b). This reduced degree of surface wettability in **1** certainly enables water molecules to move faster with less friction on their way through the aquapore. As for the average H-bond energy in the water chain, we found an even greater difference of 33% between **1** and **2**, having H-bond energies (E_2) of 5.32 and 3.97 kcal/mol, respectively. Compared to the H-bond energy of 5.65 kcal/mol in an unconstrained water chain (Figure S7c), the positions and orientations of water molecules in $(\mathbf{1}\cdot 2H_2O)_n$ are much more optimized than those in $(\mathbf{2}\cdot 2H_2O)_n$ and are in a near-optimum state, resulting in faster collective hopping of the water chain along the hollow axis.

Using Arrhenius plots of the water permeability as a function of temperature, the activation energies (E_a) for water to enter the pore were determined to be 12.06 ± 0.31 and 12.25 ± 0.25 kcal/mol for channels **1** and **2** (Figure 3d), respectively, which are only slightly smaller than that of the DOPC liposome (E_a = 12.68 ± 0.18 kcal/mol). A small difference of 1.5% in the E_a value between **1** and **2** certainly indicates a negligible contribution of the water dehydration penalty at the channel entrance to the observed huge difference in water flow rate between **1** and **2**. It might be worth mentioning that an activation energy of 12.06 kcal/mol appears to be somewhat too large for a superfast water conductor such as **1**, particularly when compared to the E_a value of 5.1 kcal/mol for AQP1 that transports 5.9×10^9 H_2O s^{-1} $channel^{-1}$.[37] At the present, we are not clear about the origin of such a contradiction. Nevertheless, since provoking different transport mechanisms (e.g., through channel or diffusion across lipids or lipid defects) cannot account for the fact that structurally near-identical channel molecules **1** and **2**, having a 15-fold difference in water transport rate, display similar E_a values, we do believe that factors other than activation energy must play equally or perhaps more critical roles in water transport.

Recently, Pohl et al. has shown that pore surface wettability (e.g., the ability of channel-lining residues to form H-bonds with water molecules) and positive charges placed around the pore entrance could contribute hundred-fold and 6-fold increases in water permeability,[11,38] respectively. The relative importance of these two factors however seems to be insignificant or absent in our current water channel system and cannot be used to explain the differential water flow rates between **1** and **2**.

Therefore, speculating on the extent of positive impacts, we believe an increased degree of freedom of water molecules and a greatly reduced deviation from the H-bonded optimum structure, both of which are a result of an enlarged pore as in **1**, are more influential than the slightly reduced wettability of interior surface on enhancing **1**-mediated water transport relative to **2**. Although these two factors cannot be quantified at the present, they may combine to account for more than 1 order of magnitude (out of a total of 15-fold) improvement in water transport over that of **2**.

High Consistency between Computed and Experimental Water Transport Values. Short helical stacks $(\mathbf{1})_6$ (31 Å long) and $(\mathbf{2})_6$ (31 Å long) as well as dimeric $(gA)_2$ (25 Å long) and (5,6)carbon nanotube (CNT, cavity diameter = 4.7 Å, 30 Å long) were solvated explicitly with 8000 to 13000 water molecules (TIP3P) in a periodic box (Figure S8). The general AMBER force field (GAFF)[39] with improved torsional parameters[40] for the aromatic aquafoldamers as well as

https://dx.doi.org/10.1021/jacs.0c02013
J. Am. Chem. Soc. 2020, 142, 10050−10058

ff14SB[41] force field for gA were employed. All systems were equilibrated in an NPT (isobaric-isothermic) ensemble at a constant temperature of 300 K, followed by the production run for 100 ns using the AMBER 18 package.[42] During the 100 ns simulation time frame, 83, 9, 22, and 624 water molecules pass through channels $(\mathbf{1})_6$, $(\mathbf{2})_6$, $(gA)_2$, and (5,6)CNT, corresponding to water transport rates of 8.3×10^8, 9.0×10^7, 2.2×10^8, and 6.2×10^9 H_2O s^{-1} $channel^{-1}$ (Table 1), respectively.

Table 1. Experimental and Computed Water Transport Rates through the Nanopores Enclosed in $(\mathbf{1})_6$, $(\mathbf{2})_6$, $(gA)_2$, and (5,6)CNT

	water permeability (P_w)		
channels	cm^3/s	water molecules/s[a]	computed values (water molecules/s)[a]
$(\mathbf{1})_6$	9.23×10^{-14}	3.0×10^9 (1.00)	8.3×10^8 (1.00)
$(\mathbf{2})_6$	0.66×10^{-14}	2.2×10^8 (0.07)	9.0×10^7 (0.11)
$(gA)_2$	1.95×10^{-14}	6.4×10^8 (0.21)	2.2×10^8 (0.27)
(5,6) CNT[b]	6.8×10^{-13}	2.3×10^{10} (7.67)	6.2×10^9 (7.47)

[a]Values in parentheses are the relative transport rates with those of $(\mathbf{1})_6$ set to 1.00. [b]Experimental value was obtained from ref 29.

Since these transport rates were obtained by simple diffusion in the absence of a concentration gradient, they are different from the experimental values obtained using 300 mM sucrose as the draw solute. Nevertheless, with both the experimental and computed water transport rates of $(\mathbf{1})_6$ set to 1.00, the relative water transport rates involving the four channels are remarkably consistent between experimental and computed values. This high consistency confirms an extraordinarily high ability of $(\mathbf{1})_6$ to mediate fast water transport at a rate of 3.0×10^9 H_2O s^{-1} $channel^{-1}$, which is 15 times that of $(\mathbf{2})_6$.

The binding energies E_1 and E_2 for (5,6)CNT were calculated to be 9.81 and 5.07 kcal/mol (Figure 3c), respectively, which, when compared to E_1 and E_2 values for **1** and **2**, are in great accord with the experimentally proven[29] and computationally verified hyperfast water transport through (5,6)CNT (Table 1).

The fact that these computational values are in excellent accord with experimental values unambiguously confirm that water molecules are transported predominantly, if not 100%, through the pore of **1**, rather than though such as lipid defects by diffusion.

Computational Estimation of Transport Selectivities of Water/Na^+, Water/K^+, and Water/Cl^-. We have further conducted a prolonged computational study of >1000 ns trajectory in order to shed some additional computational insights into **1**-mediated selectivity in terms of water/Na^+, water/K^+, and water/Cl^- (Table 2)

For calculating water/Na^+ selectivity, the simulation setup contains 8000 water molecules and 88 NaCl. Within a period of 1360 ns, 1225 water molecules passed through the channel ($\sim 8.5 \times 10^8$ water molecules/s) and 12025 water molecules entered into at least 1/8 of the channel length (~3.5 Å). Within the same period, no single ion (Na^+ or Cl^-) entered into or was found in the channel at any point of time. With estimation, the selectivity of water/NaCl is at least 1323 (= 12025/(8000/88)).

For calculating water/K^+ selectivity, the simulation setup contains 8000 water molecules and 88 KCl. Within a period of 1200 ns, 1023 water molecules passed through the channel ($\sim 9.0 \times 10^8$ water molecules/s) and 10226 water molecules entered into at least 1/8 of the channel length (~3.5 Å). Within the same period, no single ion (K^+ or Cl^-) entered into or was found in the channel at any point of time. It is estimated that the selectivity of water/KCl is at least 1125 (= 10226/(8000/88)).

Table 2. Computational Estimation of 1-Mediated Transport Selectivities of Water/Na^+, Water/K^+, and Water/Cl^-[a]

	no. of water molecules that passed the channel	no. of water molecules that entered 1/8 of the channel (~3.5 Å)	selectivity (water/MCl)
NaCl system	1225	12025	1323[b]
KCl system	1023	10226	1125[c]

[a]The simulation setup box contains 88 NaCl or 88 KCl dissolved in 8000 water molecules (~0.6 M MCl, M = Na or K). For NaCl, the simulation was run for 1360 ns; for KCl, the simulation was run for 1200 ns. [b]Value = 12025/(8000/88). [c]Value = 10226/(8000/88).

Such high selectivities in water/Na^+, water/K^+, and water/Cl^- actually are well expected since, as discussed earlier, the narrow hollow cavity of 2.8 Å contained in **1**, which is just big enough for a single water molecule, lacks binding elements for compensating the needed dehydration energies for ions to enter and pass the channel in a largely dehydrated form.

Comparative Analyses between 1 and AqpZ. Even based on a revised water transport rate of $\sim 6.0 \times 10^9$ H_2O s^{-1} $channel^{-1}$ by AqpZ recently reported by Pohl,[11] highly selective water channel **1** mediates rapid water transport at capacity as much as 50% that of AqpZ. From a crystalline 2D packing involving 1D water channels $(\mathbf{1}{\cdot}2H_2O)_n$ in its crystal structure (Figure S9a), 1D channels $(\mathbf{1}{\cdot}2H_2O)_n$ are estimated to have a rectangular cross section of 1.18 nm (W) × 1.36 nm (L). The corresponding area of 1.6 nm^2 is 18% that of the isolated AqpZ (3 nm × 3 nm)[43] or 7% that of AqpZ in a 2D crystal packing on mica (22.56 nm^2 per AqpZ, Figure S9b).[44] Therefore, in highly packed 2D crystal arrays made up of 100% $(\mathbf{1})_6$ or $(AqpZ)_4$, water channels **1** and AqpZ, in principle, could mediate water fluxes of ~200 and ~28 m^3 m^{-2} h^{-1}, respectively, with **1** outperforming AqpZ by 6 times. Moreover, compared to bulkier and more expensive $(AqpZ)_4$ having a large combined molecular weight of 95 kDa, molecular weight of $(\mathbf{1})_6$ is only 4.6 kDa. These advantageous features, when additionally considering the fact that complete artificiality of **1** shall allow simpler membrane fabrication and system integration than its protein counterparts, suggesting possible use of **1** as an active component of RO membrane.

CONCLUSION

In summary, we have demonstrated here great utility of a "sticky end"-mediated molecular strategy in the discovery of an aquaporin-like synthetic water channel **1**. Molecules of **1** are able to pile up one dimensionally to create hollow pores of 2.8 Å across, trapping single-file water chains for conducting superfast transmembrane water transport at capacity 50% that of AqpZ and with high selectivity. Given its robust helical structure, high chemical stability and scalability, as well as low cost, **1** with fascinating water transport features could be valuable for a variety of applications. This may include the making of novel biomimetic RO membranes that might form the basis for next-generation water purification technology with

https://dx.doi.org/10.1021/jacs.0c02013
J. Am. Chem. Soc. 2020, 142, 10050−10058

less energy consumption and better performance. In light of the sharp contrast in water transport performance between structurally similar channels **1** and **2**, we here propose an increased degree of freedom of water molecules and reduced deviation from the H-bonded optimum structure as another two previously overlooked yet influential factors that can be incorporated into the design consideration of synthetic water channels for improving water permeability.[11,38]

EXPERIMENTAL SECTION

Materials. All the reagents were obtained from commercial suppliers and used as received unless otherwise noted. Aqueous solutions were prepared from Milli-Q water. 1,2-Dioleoyl-*sn*-glycero-3-phosphocholine lipid (DOPC) used in this study was obtained from Avanti Polar Lipids. The CCDC number for crystal **1**·2H_2O is 1954834.

Procedure for Water Transport Study. DOPC (0.24 mL, 25 mg/mL in $CHCl_3$, Avanti Polar Lipids) and channel samples (**1**, **2**, or gA in chloroform) were mixed at different molar ratios (300:1 to 1300:1) in microtubes (2 mL). The solvent was removed by N_2 flow, and the resulting film was dried under high vacuum overnight. HEPES buffer (10 mM HEPES, 100 mM NaCl, pH = 7.0, 1.0 mL) was then added, followed by vortexing the solution for 30 s and then 10 cycles of sonication (37 kHz, power 100, 70 °C, 2.5 min) in order to maximize incorporation extent of channel molecules into membrane. A glass spatula was used if necessary to make sure the residue was fully detached from the surface of the microtube. The mixture was further subjected to 10 freeze−thaw cycles (freezing in liquid N_2 for 1 min and heating in a 55 °C water bath for 2 min) and extruded at 80 °C for 15 times. The LUVs obtained this way contain 6 mg/mL of lipids, were stored in a 4 °C fridge before use, and diluted six times with HEPES buffer to make 1 mg/mL LUV for stopped flow measurement. The particle size of LUV (120 nm) was characterized by dynamic light scattering (Zetasizer Nano, Malvern Instruments Ltd., U.K.). The water permeability measurements were conducted on a stopped-flow instrument (Chirascan circular dichroism spectrometer, Applied Photophysics, U.K.). Exposure of vesicles to three types of hypertonic osmolytes resulted in the shrinkage of the vesicles due to an outwardly directed osmotic gradient. The abrupt decrease of the vesicle size leads to an increase in light scattering intensity at a 90° angle based on the Rayleigh−Gans theorem. The changes of light scattering intensity caused by vesicle shrinkage were recorded at a wavelength of 577 nm and were fitted in the following form of single exponential function.

$$y = A\exp(-kx) + y0$$

where y = change in the light scattering, k is the exponential coefficient of the change in the light scattering, and x is time.

With the assumption that change in the light scattering intensity is proportional to the change in the vesicle volume ($\Delta V/V_0$) based on the Boyle−van't Hoff law, the osmotic permeability (P_f) in the unit of cm/s was calculated as follows:

$$P_f = k/((S/V_0) \times V_w x \Delta_{osm})$$

where k is the exponential coefficient of the change in the light scattering; S and V_0 are the initial surface area and volume of the vesicles, respectively; V_w is the molar volume of water, and Δ_{osm} is the osmolarity difference.

To calculate the true water permeability (P_w in the unit of cm^3/s) of the water channels, the $P_{f(blank)}$ value of the blank vesicle without water channels needs to be deducted from $P_{f\,(channel)}$, which was multiplied by the vesical surface area (S) and divided by the number of water channels (N) incorporated in the liposome as shown below.

$$P_w = (P_{f(channel)} - P_{f(blank)}) \times (S/N)$$

HPTS Assay for Cation Transport Study. Egg yolk L-α-phosphatidylcholine (EYPC, 1 mL, 25 mg/mL in $CHCl_3$, Avanti Polar Lipids) was added in a round-bottom flask. The solvent was removed under reduced pressure at 30 °C. After drying the resulting film under high vacuum overnight, the film was hydrated with 4-(2-hydroxyethyl)-1-piperazine-ethanesulfonic acid (HEPES) buffer solution (1 mL, 10 mM HEPES, pH = 7.0), containing a pH sensitive dye 8-hydrox-ypyrene-1,3,6-trisulfonic acid (HPTS, 1 mM), at room temperature by votexing for 60 min to give a milky suspension. The mixture was then subjected to 10 freeze−thaw cycles: freezing in liquid N_2 for 1 min and heating in a 55 °C water bath for 2 min. The vesicle suspension was extruded through polycarbonate membrane (0.1 μm) to produce a homogeneous suspension of large unilamellar vesicles (LUVs) of about 120 nm in diameter with HPTS encapsulated inside. The unencapsulated HPTS dye was separated from the LUVs using size exclusion chromatography (stationary phase, Sephadex G-50, GE Healthcare; mobile phase, HEPES buffer with pH = 7.0) and diluted with the mobile phase to yield 13 mL of 2.5 mM lipid stock solution.

The HPTS-containing LUV suspension (25 μL, 2.5 mM lipid in 10 mM HEPES buffer at pH 7.0) was added to a HEPES buffer solution (1.95 mL, 10 mM HEPES, 200 mM M_2SO_4, pH 7.0, where M^+ = Na^+ or K^+) to create a metal ion concentration gradient for the ion transport study. A solution of channel molecules (**1** at 720 μM or gA at 20 μM) in DMSO was then injected into the suspension under gentle stirring.

HPTS Assay for Anion Transport Study. The SPQ-containing LUV suspension (25 μL, 2.5 mM lipid, 200 mM $NaNO_3$) was added to a solution (1.95 mL, 200 mM NaCl) to create anion concentration gradients for the ion transport study. A solution of channel molecule **1** at 120 μM in DMSO was then injected into the suspension under gentle stirring.

Proton Transport Study Using the HPTS Assay. Egg yolk L-α-phosphatidylcholine (EYPC, 1 mL, 25 mg/mL in $CHCl_3$, Avanti Polar Lipids) was added in a round-bottom flask. The solvent was removed under reduced pressure at 30 °C. After drying the resulting film under high vacuum overnight, the film was hydrated with 4-(2-hydroxyethyl)-1-piperazine-ethanesulfonic acid (HEPES) buffer solution (1 mL, 10 mM HEPES, 100 mM NaCl, pH = 7.0), containing a pH sensitive dye 8-hydrox-ypyrene-1,3,6- trisulfonic acid (HPTS, 1 mM), at room temperature by votexing for 60 min to give a milky suspension. The mixture was then subjected to 10 freeze−thaw cycles: freezing in liquid N_2 for 1 min and heating in a 55 °C water bath for 2 min. The vesicle suspension was extruded through polycarbonate membrane (0.1 μm) to produce a homogeneous suspension of large unilamellar vesicles (LUVs) of about 120 nm in diameter with HPTS encapsulated inside. The unencapsulated HPTS dye was separated from the LUVs using size exclusion chromatography (stationary phase, Sephadex G-50, GE Healthcare; mobile phase, HEPES buffer with 100 mM NaCl, pH = 7.0) and diluted with the mobile phase to yield 13 mL of 2.5 mM lipid stock solution.

The HPTS-containing LUV suspension (25 μL, 2.5 mM lipid in 10 mM HEPES buffer containing 100 mM NaCl at pH = 7.0) was added to a HEPES buffer solution (1.95 mL, 10 mM HEPES, 100 mM MCl, pH = 8.0, where M^+ = Na^+ or K^+) to create a pH gradient for the ion transport study. A solution of channel molecules in DMSO (**1** at 720 μM or gA at 20 μM) was then injected into the suspension under gentle stirring. Upon the addition of channels, the emission of HPTS was immediately monitored at 510 nm with excitations at both 460 and 403 nm recorded simultaneously for 300 s using a fluorescence spectrophotometer (Hitachi, model F-7100, Japan) after which time an aqueous solution of Triton X-100 was immediately added to achieve the maximum change in dye fluorescence emission. The final transport trace was obtained, after subtracting background intensity at t = 0, as a ratiometric value of I_{460}/I_{403} and normalized based on the ratiometric value of I_{460}/I_{403} after addition of triton. The fractional changes R_H^+ was calculated for each curve using the normalized value of I_{460}/I_{403} at 300 s before the addition of triton, with triton with a ratiometric value of I_{460}/I_{403} at t = 0 s as 0% and that of I_{460}/I_{403} at t = 300 s (obtained after addition of triton) as 100%.

Calculation of Internal Volumes. The VolMap method in VMD were used to obtain a density map in the format of a 3-dimension grid file (grid size = 0.3 × 0.3 × 0.3 $Å^3$). The calculation of the volume of either the water chain or the cavity of the channel is carried out based

https://dx.doi.org/10.1021/jacs.0c02013
J. Am. Chem. Soc. 2020, 142, 10050−10058

on these density grids, with the volume calculated by adding up the volume of all the occupied or unoccupied grids.

For calculating the volume of the water chain, a grid with a density >0.5 is considered occupied, and the volume of the water chain is obtained by adding up the volumes of all the occupied grids. For calculating the density map of the internal pore volume in channels **1** or **2**, a grid with a density <0.2 is considered occupied, and the volume of the internal hollow pore is obtained by adding up the volumes of all the unoccupied grids. However, such calculation is a bit more complicated than calculating the volume of the water chain as one has to distinguish the unoccupied grid outside the foldamer channel and those inside the foldamer channel. Only the unoccupied grids inside the channel should be counted. Thus, we first defined a cylinder with a diameter larger than the channel pore but smaller than the outer diameter of the channel, which will enclose the channel pore of 2.8 Å in diameter and exclude most of the volume outside the channel pore. Then only the unoccupied grid inside the cylinder is added up to calculate the channel volume.

Activation Energy Measurements. To determine the activation energies for water transport, we conducted water permeability measurements at different temperatures at intervals of 5 °C between 20 and 40 °C. For these experiments, the solution reservoir and the measurement cell of the stopped-flow instrument were maintained at a set temperature by a recirculating heater/chiller (Polystat, Cole Parmer). Permeability rates through channels at varying temperatures were used to construct an Arrhenius plot.

$$\ln(k) = \ln(A) - E_\alpha/(RT)$$

where k is the exponential coefficient of the change in the light scattering; A is the pre-exponential factor; E_α is the activation energy; R is the gas constant; and T is the absolute temperature.

Molecular Dynamics Simulations. The general AMBER force field (GAFF),[39] with improved torsional parameters for the aromatic aquafoldamers[40] as well as the ff14SB[41] force field for gA, was used in all of the simulations. Each simulated system contains a water channel (**1**, **2**, gA, or CNT) solvated in ∼8−13K water molecules in a periodic box. The systems were initially equilibrated for 3 ns in an NPT ensemble at a constant temperature of 300 K and a pressure of 1 atm. For the first 2 ns of NPT, the channel is constrained for water molecules to disperse into the channel and reach equilibrium. Then all constraints are removed in subsequent simulations for all systems except for gA, in which a few constrains were added to keep the "head-to-head" dimer together in the aqueous environment. The constraints include distance between the center of masses of the Cα atoms of the two helices, distance between the first C atoms of the two helices, and the hydrogen bond between the first amide NH of each helix to the fifth amide C═O of the other helix. The production run of each system is carried out in an NVT ensemble at a constant temperature of 300 K for at least 100 ns. All simulations were carried out using the AMBER 18 package.[42] For estimating **1**-mediated selectivity in terms of water/Na^+, water/K^+, and water/Cl^-, the simulation setup box contains 88 NaCl or 88 KCl dissolved in 8000 water molecules (∼0.6 M MCl, M = Na or K). For NaCl, the simulation was run for 1360 ns; for KCl, the simulation was run for 1200 ns.

■ ASSOCIATED CONTENT

Supporting Information

The Supporting Information is available free of charge at https://pubs.acs.org/doi/10.1021/jacs.0c02013.

Full set of characterization data including ion transport study, CF assay, and computational details (PDF)

Crystallographic details of **1** (CIF)

■ AUTHOR INFORMATION

Corresponding Author

Huaqiang Zeng − *The NanoBio Lab, Singapore 138669;* orcid.org/0000-0002-8246-2000; Email: hqzeng@nbl.a-star.edu.sg

Authors

Jie Shen − *The NanoBio Lab, Singapore 138669*

Ruijuan Ye − *Department of Chemical and Biomolecular Engineering, National University of Singapore, Singapore 117585*

Alyssa Romanies − *Department of Chemistry & Biochemistry and the West Center for Computational Chemistry and Drug Design, University of the Sciences in Philadelphia, Philadelphia, Pennsylvania 19104, United States*

Arundhati Roy − *The NanoBio Lab, Singapore 138669*

Feng Chen − *The NanoBio Lab, Singapore 138669*

Changliang Ren − *The NanoBio Lab, Singapore 138669*

Zhiwei Liu − *Department of Chemistry & Biochemistry and the West Center for Computational Chemistry and Drug Design, University of the Sciences in Philadelphia, Philadelphia, Pennsylvania 19104, United States*

Complete contact information is available at: https://pubs.acs.org/10.1021/jacs.0c02013

Notes

The authors declare no competing financial interest.

■ ACKNOWLEDGMENTS

This work was supported by the Nanobio Lab (Biomedical Research Council, Agency for Science, Technology and Research, Singapore), the Singapore National Research Foundation under its Environment and Water Research Programme and administered by PUB and NSF CHE-1710466 grant for MD simulation.

■ REFERENCES

(1) Mekonnen, M. M.; Hoekstra, A. Y. Four billion people facing severe water scarcity. *Sci. Adv.* **2016**, *2*, No. e1500323.

(2) Hoekstra, A. Y.; Wiedmann, T. O. Humanity's unsustainable environmental footprint. *Science* **2014**, *344*, 1114.

(3) Eliasson, J. The rising pressure of global water shortages. *Nature* **2015**, *517*, 6.

(4) Imbrogno, J.; Belfort, G. Membrane Desalination: Where Are We, and What Can We Learn from Fundamentals? *Annu. Rev. Chem. Biomol. Eng.* **2016**, *7*, 29.

(5) Petersen, R. J. Composite reverse osmosis and nanofiltration membranes. *J. Membr. Sci.* **1993**, *83*, 81.

(6) Greenlee, L. F.; Lawler, D. F.; Freeman, B. D.; Marrot, B.; Moulin, P. Reverse osmosis desalination: Water sources, technology, and today's challenges. *Water Res.* **2009**, *43*, 2317.

(7) Murata, K.; Mitsuoka, K.; Hirai, T.; Walz, T.; Agre, P.; Heymann, J. B.; Engel, A.; Fujiyoshi, Y. Structural determinants of water permeation through aquaporin-1. *Nature* **2000**, *407*, 599.

(8) Tajkhorshid, E.; Nollert, P.; Jensen, M. Ø.; Miercke, L. J. W.; O'Connell, J.; Stroud, R. M.; Schulten, K. Control of the Selectivity of the Aquaporin Water Channel Family by Global Orientational Tuning. *Science* **2002**, *296*, 525.

(9) Takata, K.; Matsuzaki, T.; Tajika, Y. Aquaporins: water channel proteins of the cell membrane. *Prog. Histochem. Cytochem.* **2004**, *39*, 1.

(10) Borgnia, M. J.; Kozono, D.; Calamita, G.; Maloney, P. C.; Agre, P. Functional reconstitution and characterization of AqpZ, the E. coli water channel protein. *J. Mol. Biol.* **1999**, *291*, 1169.

(11) Horner, A.; Siligan, C.; Cornean, A.; Pohl, P. Positively charged residues at the channel mouth boost single-file water flow. *Faraday Discuss.* **2018**, *209*, 55.
(12) Elimelech, M.; Phillip, W. A. The future of seawater desalination: energy, technology, and the environment. *Science* **2011**, *333*, 712.
(13) Barboiu, M.; Gilles, A. From Natural to Bioassisted and Biomimetic Artificial Water Channel Systems. *Acc. Chem. Res.* **2013**, *46*, 2814.
(14) Fane, A. G.; Wang, R.; Hu, M. X. Synthetic Membranes for Water Purification: Status and Future. *Angew. Chem., Int. Ed.* **2015**, *54*, 3368.
(15) Werber, J. R.; Osuji, C. O.; Elimelech, M. Materials for next-generation desalination and water purification membranes. *Nat. Rev. Mater.* **2016**, *1*, 16018.
(16) Wagh, P.; Escobar, I. Biomimetic and bioinspired membranes for water purification: A critical review and future directions. *Environ. Prog. Sustainable Energy* **2019**, *38*, e13215.
(17) Song, W.; Kumar, M. Artificial water channels: toward and beyond desalination. *Curr. Opin. Chem. Eng.* **2019**, *25*, 9.
(18) Huo, Y. P.; Zeng, H. Q. Sticky"-Ends-Guided Creation of Functional Hollow Nanopores for Guest Encapsulation and Water Transport. *Acc. Chem. Res.* **2016**, *49*, 922.
(19) Werber, J. R.; Elimelech, M. Permselectivity limits of biomimetic desalination membranes. *Sci. Adv.* **2018**, *4*, No. eaar8266.
(20) Kaucher, M. S.; Peterca, M.; Dulcey, A. E.; Kim, A. J.; Vinogradov, S. A.; Hammer, D. A.; Heiney, P. A.; Percec, V. Selective transport of water mediated by porous dendritic dipeptides. *J. Am. Chem. Soc.* **2007**, *129*, 11698.
(21) Le Duc, Y.; Michau, M.; Gilles, A.; Gence, V.; Legrand, Y.-M.; van der Lee, A.; Tingry, S.; Barboiu, M. Imidazole-Quartet Water and Proton Dipolar Channels. *Angew. Chem., Int. Ed.* **2011**, *50*, 11366.
(22) Zhou, X. B.; Liu, G. D.; Yamato, K.; Shen, Y.; Cheng, R. X.; Wei, X. X.; Bai, W. L.; Gao, Y.; Li, H.; Liu, Y.; Liu, F. T.; Czajkowsky, D. M.; Wang, J. F.; Dabney, M. J.; Cai, Z. H.; Hu, J.; Bright, F. V.; He, L.; Zeng, X. C.; Shao, Z. F.; Gong, B. Self-assembling subnanometer pores with unusual mass-transport properties. *Nat. Commun.* **2012**, *3*, 949.
(23) Hu, C. B.; Chen, Z. X.; Tang, G. F.; Hou, J. L.; Li, Z. T. Single-Molecular Artificial Transmembrane Water Channels. *J. Am. Chem. Soc.* **2012**, *134*, 8384.
(24) Licsandru, E.; Kocsis, I.; Shen, Y.-x.; Murail, S.; Legrand, Y.-M.; van der Lee, A.; Tsai, D.; Baaden, M.; Kumar, M.; Barboiu, M. Salt-Excluding Artificial Water Channels Exhibiting Enhanced Dipolar Water and Proton Translocation. *J. Am. Chem. Soc.* **2016**, *138*, 5403.
(25) Zhao, H. Q.; Sheng, S.; Hong, Y. H.; Zeng, H. Q. Proton Gradient-Induced Water Transport Mediated by Water Wires inside Narrow Aquapores of Aquafoldamer Molecules. *J. Am. Chem. Soc.* **2014**, *136*, 14270.
(26) Shen, Y.-x.; Si, W.; Erbakan, M.; Decker, K.; De Zorzi, R.; Saboe, P. O.; Kang, Y. J.; Majd, S.; Butler, P. J.; Walz, T.; Aksimentiev, A.; Hou, J.-l.; Kumar, M. Highly permeable artificial water channels that can self-assemble into two-dimensional arrays. *Proc. Natl. Acad. Sci. U. S. A.* **2015**, *112*, 9810.
(27) Kocsis, I.; Sorci, M.; Vanselous, H.; Murail, S.; Sanders, S. E.; Licsandru, E.; Legrand, Y.-M.; van der Lee, A.; Baaden, M.; Petersen, P. B.; Belfort, G.; Barboiu, M. Oriented chiral water wires in artificial transmembrane channels. *Sci. Adv.* **2018**, *4*, No. eaao5603.
(28) Song, W.; Joshi, H.; Chowdhury, R.; Najem, J. S.; Shen, Y.-x.; Lang, C.; Henderson, C. B.; Tu, Y.-M.; Farell, M.; Pitz, M. E.; Maranas, C. D.; Cremer, P. S.; Hickey, R. J.; Sarles, S. A.; Hou, J.-l.; Aksimentiev, A.; Kumar, M. Artificial water channels enable fast and selective water permeation through water-wire networks. *Nat. Nanotechnol.* **2020**, *15*, 73.
(29) Tunuguntla, R. H.; Henley, R. Y.; Yao, Y.-C.; Pham, T. A.; Wanunu, M.; Noy, A. Enhanced water permeability and tunable ion selectivity in subnanometer carbon nanotube porins. *Science* **2017**, *357*, 792.
(30) Shen, J.; Fan, J.; Ye, R. J.; Li, N.; Mu, Y.; Zeng, H. Q. Polypyridine-Based Helical Amide Foldamer Channels: Rapid Transport of Water and Protons with High Ion Rejection. *Angew. Chem., Int. Ed.* **2020**, DOI: 10.1002/anie.202003512.
(31) Zhao, H. Q.; Ong, W. Q.; Zhou, F.; Fang, X.; Chen, X. Y.; Li, S. F. Y.; Su, H. B.; Cho, N.-J.; Zeng, H. Q. Chiral crystallization of aromatic helical foldamers via complementarities in shape and end functionalities. *Chem. Sci.* **2012**, *3*, 2042.
(32) Ren, C.; Ding, X.; Roy, A.; Shen, J.; Zhou, S.; Chen, F.; Yau Li, S. F.; Ren, H.; Yang, Y. Y.; Zeng, H. A halogen bond-mediated highly active artificial chloride channel with high anticancer activity. *Chem. Sci.* **2018**, *9*, 4044.
(33) The water transport rate of channel **1** was caculated to be 1.4×10^9 H_2O s^{-1} $channel^{-1}$ when calculated using Pohl's new equation. For this new equation, see Hannesschläger, C.; Barta, T.; Siligan, C.; Horner, A. Quantification of Water Flux in Vesicular Systems. *Sci. Rep.* **2018**, *8*, 8516.
(34) Pohl, P.; Saparov, S. M. Solvent drag across gramicidin channels demonstrated by microelectrodes. *Biophys. J.* **2000**, *78*, 2426.
(35) Meinild, A. K.; Klaerke, D. A.; Zeuthen, T. Bidirectional water fluxes and specificity for small hydrophilic molecules in aquaporins 0–5. *J. Biol. Chem.* **1998**, *273*, 32446.
(36) Verkman, A. S.; Takla, R.; Sefton, B.; Basbaum, C.; Widdicombe, J. H. Quantitative fluorescence measurement of chloride transport mechanisms in phospholipid vesicles. *Biochemistry* **1989**, *28*, 4240.
(37) Horner, A.; Pohl, P. Comment on Enhanced water permeability and tunable ion selectivity in subnanometer carbon nanotube porins. *Science* **2018**, *359*, No. eaap9173.
(38) Horner, A.; Zocher, F.; Preiner, J.; Ollinger, N.; Siligan, C.; Akimov, S. A.; Pohl, P. The mobility of single-file water molecules is governed by the number of H-bonds they may form with channel-lining residues. *Sci. Adv.* **2015**, *1*, No. e1400083.
(39) Wang, J.; Wolf, R. M.; Caldwell, J. W.; Kollman, P. A.; Case, D. A. Development and testing of a general amber force field. *J. Comput. Chem.* **2004**, *25*, 1157.
(40) Liu, Z.; Abramyan, A. M.; Pophristic, V. Helical arylamide foldamers: structure prediction by molecular dynamics simulations. *New J. Chem.* **2015**, *39*, 3229.
(41) Maier, J. A.; Martinez, C.; Kasavajhala, K.; Wickstrom, L.; Hauser, K. E.; Simmerling, C. ff14SB: Improving the Accuracy of Protein Side Chain and Backbone Parameters from ff99SB. *J. Chem. Theory Comput.* **2015**, *11*, 3696.
(42) Case, D. A.; Ben-Shalom, I. Y.; Brozell, S. R.; Cerutti, D. S.; T.E. Cheatham, I.; Cruzeiro, V. W. D.; Darden, T. A.; Duke, R. E.; Ghoreishi, D.; Gilson, M. K.; Gohlke, H.; Goetz, A. W.; Greene, D.; Harris, R.; Homeyer, N.; Izadi, S.; Kovalenko, A.; Kurtzman, T.; Lee, T. S.; LeGrand, S.; Li, P.; Lin, C.; Liu, J.; Luchko, T.; Luo, R.; Mermelstein, D. J.; Merz, K. M.; Miao, Y.; Monard, G.; Nguyen, C.; Nguyen, H.; Omelyan, I.; Onufriev, A.; Pan, F.; Qi, R.; Roe, D. R.; Roitberg, A.; Sagui, C.; Schott-Verdugo, S.; Shen, J.; Simmerling, C. L.; Smith, J.; Salomon-Ferrer, R.; Swails, J.; Walker, R. C.; Wang, J.; Wei, H.; Wolf, R. M.; Wu, X.; Xiao, L.; York, D. M.; Kollman, P. A. *AMBER 2018*; University of California, San Francisco: San Francisco, CA, 2018.
(43) Jiang, J.; Daniels, B. V.; Fu, D. Crystal Structure of AqpZ Tetramer Reveals Two Distinct Arg-189 Conformations Associated with Water Permeation through the Narrowest Constriction of the Water-conducting Channel. *J. Biol. Chem.* **2006**, *281*, 454.
(44) Scheuring, S.; Ringler, P.; Borgnia, M.; Stahlberg, H.; Muller, D. J.; Agre, P.; Engel, A. High resolution AFM topographs of the Escherichia coli water channel aquaporin Z. *EMBO J.* **1999**, *18*, 4981.